Nanotechnology **24** (2013) 424009 (9pp) doi:10.1088/0957-4484/24/42/424009

In situ Raman spectroscopy of $LiFePO_4$: size and morphology dependence during charge and self-discharge

Jing Wu[1], Gopi Krishna Phani Dathar[2], Chunwen Sun[3], Murali G Theivanayagam[4], Danielle Applestone[5], Anthony G Dylla[1], Arumugam Manthiram[4], Graeme Henkelman[1], John B Goodenough[6] and Keith J Stevenson[1]

[1] Department of Chemistry and Biochemistry, University of Texas at Austin, Austin, TX, USA
[2] Center for Nanophase Materials Sciences, Oak Ridge National Laboratory, Oak Ridge, TN, USA
[3] Institute of Physics, Chinese Academy of Sciences, Beijing, People's Republic of China
[4] Texas Materials Institute, University of Texas at Austin, Austin, TX, USA
[5] Otherlab Incorporated, San Francisco, CA, USA
[6] Materials Science and Engineering Program, University of Texas at Austin, Austin, TX, USA

E-mail: stevenson@cm.utexas.edu

Received 1 February 2013, in final form 14 April 2013
Published 25 September 2013
Online at stacks.iop.org/Nano/24/424009

Abstract
Previous studies of the size dependent properties of $LiFePO_4$ have focused on the diffusion rate or phase transformation pathways by bulk analysis techniques such as x-ray diffraction (XRD), neutron diffraction and electrochemistry. In this work, *in situ* Raman spectroscopy was used to study the surface phase change during charge and self-discharge on a more localized scale for three morphologies of $LiFePO_4$: (1) 25 ± 6 nm width nanorods, (2) 225 ± 6 nm width nanorods and (3) ~ 2 μm porous microspheres. Both the large nanorod and microsphere geometries showed incomplete delithiation at the end of charge, which was most likely caused by anti-site defects along the 1D diffusion channels in the bulk of the larger particles. Based on the *in situ* Raman measurements, all of the morphologies studied exhibited self-discharge with time. Among them, the smallest $FePO_4$ particles self-discharged (lithiated) the fastest. While nanostructuring $LiFePO_4$ can offer advantages in terms of lowering anti-site defects within particles, it also creates new problems due to high surface energies that allow self-discharge. The *in situ* Raman spectroscopy also showed that carbon coating did not provide significant improvement to the stability of the lithiated particles.

(Some figures may appear in colour only in the online journal)

1. Introduction

Li-ion batteries have received considerable attention not only for portable electronics but also larger scale applications such as energy storage systems for intermittent renewable energy sources like wind and solar energy and electric powered vehicles. These larger scale applications will require new battery materials with lower cost, higher energy density, thermal stability, low environmental impact and faster charge/discharge rates. $LiFePO_4$ has become an attractive cathode material for the next generation lithium-ion battery since it was introduced by Goodenough and co-workers more than 15 years ago [1]. Despite the proven benefits of $LiFePO_4$ such as high theoretic capacity, low cost and good thermal stability, the performance of $LiFePO_4$ batteries is hindered by its low electronic and ionic conductivities. Efforts have been made to overcome poor conductivity by shrinking the dimensions of the $LiFePO_4$ to the nanoscale. The reduced dimensions shorten diffusion pathways for Li^+ and electrons resulting in increased conductivity. Smaller

particles also decrease defect density which is critical to a material such as $LiFePO_4$ that exhibits a one-dimensional Li^+ diffusion mechanism [2]. Several groups have reported improved Li^+ kinetics and capacity as particle size is reduced [3–5]. One drawback of nanoscaling a cathode material such as $LiFePO_4$ is that smaller particle sizes can lead to lower stability due to increased surface energy. Previous work has focused on the size related properties of the bulk material including the diffusion rate, diffusion length and the formation of solid solution at small particle sizes [6]. To our knowledge, the stability of smaller particles, especially the surface stability, has not been fully explored. Studies of $LiFePO_4$ phase change upon Li^+ extraction and insertion have been performed largely by 'bulk' ensemble averaging analytical techniques including XRD [7, 8], neutron diffraction [9] and electrochemistry [10, 11]. While these studies provide important information on diffusion rates and phase transformation pathways, they are limited in revealing surface related properties of nanoparticles. In this study we use *in situ* Raman spectroscopy along with calculated Raman spectra to explore the surface properties and reactivity of several morphologies of $LiFePO_4$.

Paques-Ledent and Tarte's early study on olivine materials showed no change of space group (*Pnma*, D_{2h}^{16}) or selection rules on the two-phase reaction from $LiFePO_4$ to $FePO_4$ [12]. The observed vibrational spectra differences are solely induced by the removal of Li^+ coordinated to the oxygen atoms in the PO_4^{3-}, which causes a distortion of the tetrahedra. As a result, the vibrations of PO_4^{3-} are extremely sensitive to the interactions of nearby lithium ions. They reported observable Raman active vibrational modes in the range of 350–1200 cm^{-1} and external modes below 350 cm^{-1} for $LiFePO_4$, which were all shifted upon removal of Li^+.

In addition to the previous work, Burba and Frech explored the Raman spectra of chemically delithiated $LiFePO_4$ as a function of Li content, Li_xFePO_4 [17]. Their results established how the Raman spectra changed with the distortion of PO_4^{3-} tetrahedral upon the partial and complete removal of Li^+ from the lattice.

In this work, Raman spectroscopy is used as an *in situ* spectroelectrochemical probe of surface properties of $LiFePO_4$ of different particle sizes and morphologies. The 1D Li-ion transport channel in $LiFePO_4$ runs along the *b*-axis and is perpendicular to the surface plane of a rod-shaped particle. These nanorods are ideal for study of size dependent surface properties without the concern of diffusion rate differences between channels, which has been reported to be very fast for small particles according to a domino-cascade model but not applicable for larger particles. The rods used in this study were previously reported by Manthiram *et al* who used a microwave assisted solvothermal and hydrothermal synthesis to obtain $LiFePO_4$ nanorods [5]. We also chose a monodisperse porous microsphere $LiFePO_4$ morphology for this study [18]. This particle has an overall larger size (∼2 μm), but with flower-like porous microstructure for increased surface area that may allow for enhanced charge transfer kinetics. In addition to experiments, density functional theory (DFT) was used to calculate and characterize the vibrational modes of $LiFePO_4$ and $FePO_4$. Those calculations were compared with Raman measurements to identify the modes sensitive to delithiation.

2. Methods

2.1. Experimental

Three morphologies of $LiFePO_4$ were prepared by methods described elsewhere [5, 18]: small (25 ± 6 nm width and up to 100 nm length), large (225 ± 6 nm width and up to 300 nm length) nanorods and monodisperse porous microspheres (with and without carbon coating). $LiFePO_4$ cathodes were prepared by mixing $LiFePO_4$, Super P carbon (Timcal) and PTFE (Sigma-Aldrich) (mass ratio: 80%:12%:8%). For *ex situ* experiments, the $LiFePO_4$ was mixed with 10% PVDF and 10% Super P to make a slurry that was drop cast onto a 1 cm^2 glassy carbon substrate. The prepared cathodes were then dried at 90 °C in a vacuum oven overnight.

The *in situ* Raman cell is design is shown in figure 1. A 2 mm hole was drilled through the back of a 2032 coin cell and a piece of glass window was attached onto the hole by epoxy. The exposed epoxy was isolated with PVDF coating from the interior of the battery. Al foil was used as current collector, 1.0 M $LiPF_6$/DEC + EC (1:1, Novolyte) as electrolyte and Li metal (Aldrich) as both the reference and counter-electrode.

All electrochemical tests were performed using an EG&G 263A potentiostat/galvanostat at a charge rate of 0.07 C to 4.3 V in the *in situ* experiments. The *ex situ* experiment was performed on a three electrode system using Li metal as reference and counter-electrodes at a charge rate of 0.05 C. *In situ* Raman spectra were acquired using a Renishaw inVia Microscope equipped with a 50× long working distance objective and a 514.5 nm Ar^+ laser. Because $LiFePO_4$ is sensitive to heating from incident laser power [19], the total power was adjusted below 10 mW and 3 spectra were obtained in sequence before measurement to ensure no photothermal damage was made to the sample.

2.2. Computational

Initial structures for $LiFePO_4$ and $FePO_4$ used in the density functional theory (DFT) calculations were obtained from the ICSD database. Structure optimization was followed by finite displacement calculations to obtain the normal modes of vibration. Total energy calculations were performed using plane-wave DFT as implemented in the Vienna *ab initio* simulation package (VASP) [13, 14]. A plane-wave cutoff of 400 eV was used to represent the electronic states and a single gamma point was used to sample the Brillouin zone. Ferromagnetic spins were initialized on Fe centers; all calculations were spin polarized. The valence electrons were described by Kohn–Sham one electron orbitals, and core electrons with projector augmented wave based pseudopotentials.

Since pure DFT fails to localize electrons on Fe metal centers, DFT + U or a hybrid DFT method has to be used. Vibrational calculations using DFT + U resulted in softer modes compared to experiment and the maximum

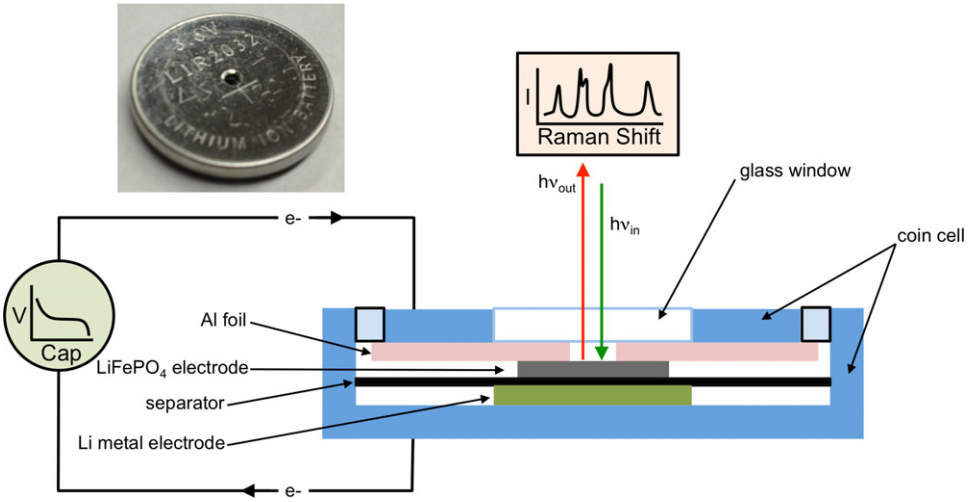

Figure 1. Modified coin cell design for *in situ* Raman spectroscopy.

deviation between the experiment and theory is on the order of 70 cm^{-1}. Hence a hybrid method was used to calculate the total energy as well as its derivatives with respect to atomic displacements. In the hybrid DFT method, the exchange–correlation (XC) contribution to DFT was calculated using Heyd–Scuseria–Ernzerhof (HSE) functional [15], in which the total exchange is comprised of (exact) Hartree–Fock and that of the Perdew–Burke–Ernzerhof (PBE) generalized gradient approximation (GGA) terms. The exact exchange term is only evaluated over a short-range; the GGA form replaces the slowly decaying long-range part of the coulomb potential. The range separation parameter $\mu = 0.2$ $Å^{-1}$ was chosen to match the HSE06 functional [16].

Vibrational modes were calculated by finite displacement of the ions by a small amount (0.001 Å) from their minimum energy positions. The Hessian matrix was calculated from the derivatives of the force with respect to displacement. The Eigen vectors of the Hessian matrix are the normal modes of vibration and the Eigen values are the normal mode frequencies. The character of the normal modes was determined from the point group symmetry of olivines.

3. Results and discussion

3.1. Ex situ Raman spectra and vibrational analysis

A Raman study of chemically delithiated Li_xFePO_4 by Burba and Frech provided a basis for the *in situ* spectroelectrochemical study of $LiFePO_4$ cathodes [17]. *Ex situ* Raman measurements were conducted to compare the electrochemically delithiated $LiFePO_4$ with results in literature before performing the *in situ* spectroelectrochemical measurements. Small $LiFePO_4$ was chosen for the *ex situ* Raman study because they contain less defects and provide more complete Li^+ extraction. The cathode was thoroughly rinsed with dimethyl carbonate and dried under argon after being charged to 4.3 V at a rate of 0.05 C. A second Raman spectrum was obtained under the same condition. The observed Raman spectra and the calculated values are shown in figure 2 and table 1, respectively. Because of the small particle size, not all the external and internal modes of $LiFePO_4$ previously reported are observed in the original electrode. Still, the most intense symmetric stretching peak at 949 cm^{-1} can be clearly identified as well as weak asymmetric stretching peaks at 995 and 1067 cm^{-1} indicating non-distorted PO_4^{3-} tetrahedra in the pristine $LiFePO_4$ [12]. After full delithiation by slow charging to 4.3 V, the Raman peaks become more intense due to the lower electronic conductivity so that both external and bending modes can be observed in the $FePO_4$ spectrum and a series of new modes appear as a result of strong PO_4^{3-} distortion [20]. The stretching modes at 908, 959, 1068 and 1126 cm^{-1}, bending modes at 487, 588, 655, and 691 cm^{-1} and external modes at 175, 244, 305, and 335 cm^{-1} all agree with those of chemically delithiated $FePO_4$ [17, 21].

Olivine phosphates belong to the space group *Pnma* (D_{2h}^{16} point group). The unit cell of $LiFePO_4$ has four formula units with Li^+, Fe^{2+} cations and a PO_4^{3-} anion. The internal modes refer to vibrations of the PO_4^{3-} anion and external modes refer to the coupled motion of the Fe^{2+} and PO_4^{3-} groups. A normal mode analysis of $LiFePO_4$ has been previously reported in literature [17, 22–24]. The normal modes are classified as $\Gamma = 11A_g + 7B_{1g} + 11B_{2g} + 7B_{3g} + 13B_{1u} + 9B_{2u} + 13B_{3u} + 10A_u$. Out of the 81 optical modes, 36 are Raman active, 45 are infrared (IR) active and 10 are silent.

The calculated normal mode frequencies of $LiFePO_4$ agree fairly well with the measured Raman modes with a maximum deviation of 33 cm^{-1}. The modes above 900 cm^{-1} correspond to the stretching of P–O bonds and the modes in the 593–637 cm^{-1} range correspond to O–P–O bending internal to the PO_4^{3-} anion. The bands at 1023, 1102, and 953 cm^{-1} are attributed to the anti-symmetric stretch (ν_3) and symmetric stretch (ν_1) of the P–O bonds. The bands at 637 cm^{-1} (A_g) and 628 cm^{-1} (B_{2g}), and the four modes in the range 593–612 cm^{-1} are attributed to the symmetric bend (ν_2) and anti-symmetric bend (ν_4) of the

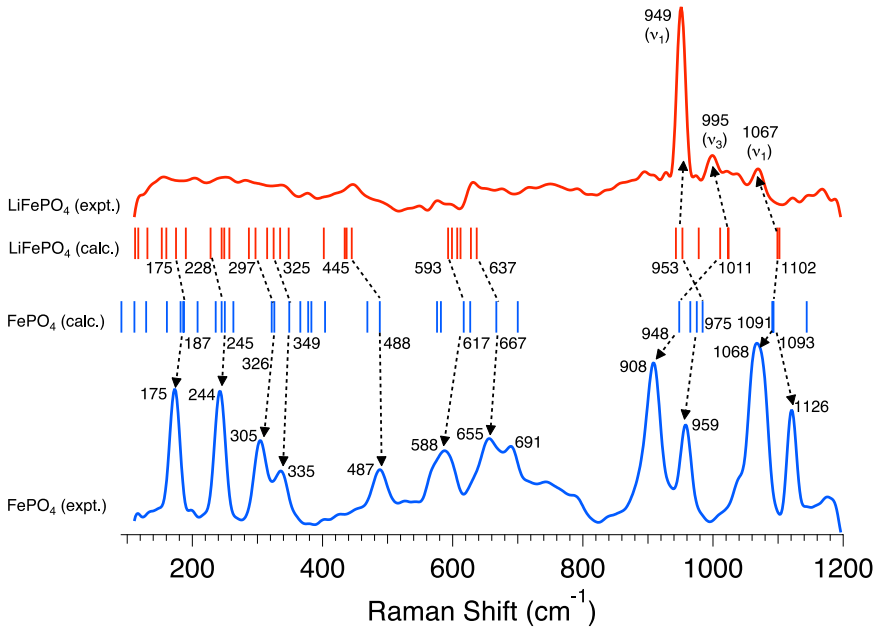

Figure 2. *Ex situ* Raman spectra of initial (red) and charged (blue) small $LiFePO_4$ nanoparticles compared to hybrid DFT (HSE06) calculated values (vertical lines).

Table 1. Calculated Raman modes of $LiFePO_4$ and $FePO_4$ with assigned vibrational mode based on the point group analysis. The values in parentheses indicate measured values in this study.

Raman active modes								
	$LiFePO_4$ (cm^{-1})				$FePO_4$ (cm^{-1})			
Vibration/character	A_g	B_{1g}	B_{2g}	B_{3g}	A_g	B_{1g}	B_{2g}	B_{3g}
Asymm. stretch PO_4^{3-} (ν_3)	1102 (1067)	1011	1099	978	1093 (1126) 1091 (1068)	965	1144 (908) 1092	948
	1023 (995)		1024					
Symm. stretch PO_4^{3-} (ν_1)	953 (949)	—	943	—	975 (959)	—	984	
Symm. bend PO_4^{3-} (ν_2)	637	—	628	—	667 (665)	—	700	
Asymm. bend PO_4^{3-} (ν_4)	593	612	599	607	617 (588)	576	627	582
Li cage/asymm. bend PO_4^{3-}	445	402	434	437	488 (487)	383	469	378
Fe–O	325	315	348	335	349 (335)	322	404	
Trans. Fe + PO_4^{3-}	297	245	287	257	326 (306)	263	366	236
	228		249		245 (244)		250	
Trans + libr. Fe + PO_4^{3-}		190		160		186		129
Trans. Fe	175	153	131	117	187 (175)	161	208	91
	112		83		111		182	

O–P–O angles. The four modes between 402 and 445 cm^{-1} correspond to the lithium cage modes with translating Li^+ and breathing cage surrounded by O^{2-} ions. The bands below 400 cm^{-1} correspond to translational motion of Fe and coupled translation and vibrational motion of Fe and PO_4^{3-}.

The number of Raman modes in $FePO_4$ is similar to $LiFePO_4$ but delithiation of $LiFePO_4$ or lithiation of $FePO_4$ results in changes to both the amplitude and position of peaks in the Raman spectrum. Such changes can be used to characterize the lithiation/delithiation in olivine phosphates.

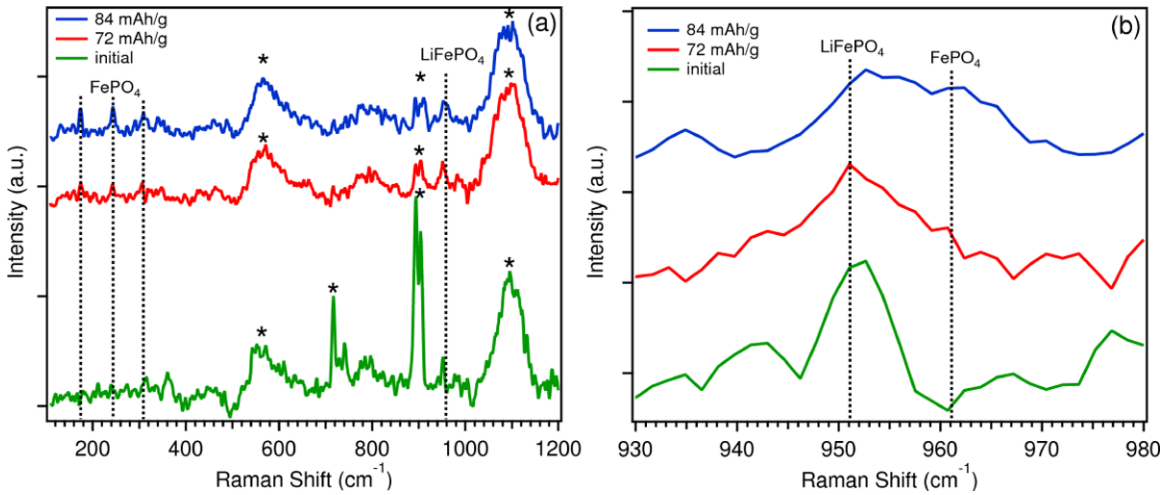

Figure 3. *In situ* Raman spectra of $LiFePO_4$ during galvanostatic charging (a), and an enlargement of the ν_1 region (b). Asterisks denote bands due to electrolyte.

The calculated modes of $FePO_4$ are also listed in table 1 and shown in figure 2. Similar to $LiFePO_4$, fair agreement between the calculated and measured modes is observed for $FePO_4$ with a maximum deviation of 30 cm^{-1}.

Shifts in the internal modes can be used to explain the new peaks in the measured Raman spectrum of $FePO_4$. The peak at 1102 cm^{-1}, corresponding to the symmetric stretch (ν_1) in $LiFePO_4$, shifts to lower frequencies and splits to form two peaks at 1093 and 1091 cm^{-1}. The peaks at 1023 cm^{-1} (A_g) and 1024 cm^{-1} (B_{2g}), corresponding to anti-symmetric stretch (ν_3), disappear in the $FePO_4$ spectrum. The other peaks at 1011 and 978 cm^{-1} (B_{1g} and B_{3g}) red-shift to 965 and 948 cm^{-1}. The symmetric stretch peak at 953 cm^{-1} blue-shifts to 975 cm^{-1}. The new split peak at 1100 cm^{-1} is attributed to the anti-symmetric stretch and the new peak at 908 cm^{-1} is due to the red-shift of one of the anti-symmetric stretching modes. The symmetric and asymmetric bend modes are shifted to higher frequencies upon delithiation. Comparing the measured and calculated modes, the peaks between 588 and 691 cm^{-1} correspond to the symmetric and anti-symmetric bend of O–P–O angles. The peak at 488 cm^{-1} corresponds to Li cage modes in $LiFePO_4$ that are blue-shifted in $FePO_4$.

The low frequency modes (<400 cm^{-1}) are of particular interest as the differences between the lithiated and delithiated materials are prominent. The lower frequencies correspond to translation of Fe and coupled translation and vibrational motion of Fe and PO_4^{3-}. A minimal shift is seen in the low frequency modes when comparing the experimental spectra of $LiFePO_4$ and $FePO_4$. Though assignment to the calculated modes, the peaks at 175 cm^{-1}, 244 cm^{-1} and 305 cm^{-1}, and 335 cm^{-1} correspond to translation of Fe, coupled translation of Fe and PO_4^{3-} and Fe–O vibrations, respectively.

3.2. In situ Raman study during charging

Three morphologies of $LiFePO_4$ were chosen for *in situ* Raman analysis: nanoparticles (small), microparticles (large) and bulk particles with porous nanomorphology on the surface (microsphere). For the *in situ* spectroelectrochemical study, $LiFePO_4$ cathodes were sealed into the Raman cell as described in figure 1. The $LiFePO_4$ *in situ* cells discharged at the characteristic ~3.5 V, which confirmed that the epoxy glued glass window did not contaminate the electrolyte or cause air leakage. Total charge capacity of the small $LiFePO_4$ was 84 mAh g^{-1}, which is reasonable for the non-carbon coated $LiFePO_4$. The *in situ* Raman spectra of small $LiFePO_4$ during charging are shown in figure 3(a). The observed peak intensities of $LiFePO_4$ cathode are attenuated by scattering and absorption from both electrolyte and the glass window, leaving only the PO_4^{3-} ν_1 mode at 951 cm^{-1} detectable. In addition, the electrolyte solution provided a series of broad peaks at 500–670, 706–763, 879–922 cm^{-1} and 1026–1159 cm^{-1}. As a result, only the <400 cm^{-1} external mode region is presented as the existence of $FePO_4$ and 930–970 cm^{-1} PO_4^{3-} ν_1 regions for the existence of both $LiFePO_4$ and $FePO_4$. As shown in figure 3(a), after a total of 72 mAh g^{-1} was charged, peaks at 175 and 244 cm^{-1} started to appear signifying a phase change from $LiFePO_4$ to $FePO_4$ on the surface of the electrode exposed to the laser. The intensity of external modes grew continuously and reached the maximum at the end of charge. Because of the decreasing conductivity upon the removal of Li^+, the intensity increase alone cannot determine the relative amount of $FePO_4$. As shown in figure 3(b), the 930–970 cm^{-1} region is still dominated by the $LiFePO_4$ symmetric stretch at 951 cm^{-1} at 72 mAh g^{-1}. The amount of $FePO_4$ increases continuously as indicated by the peak broadening near 960 cm^{-1}. At the end of charge, there is still an amount of $LiFePO_4$ that can be detected indicting an incomplete delithiation of the cathode, which is consistent with the lower discharge capacity.

The mixed phase of $LiFePO_4$ and $FePO_4$ could be the result of a mixture of pure $LiFePO_4$ and $FePO_4$ particles or incomplete delithiation of individual $LiFePO_4$ particles. Delmas *et al* reported that, for ~100 nm $LiFePO_4$ particles, Li^+ transport between 1D channels was every fast, which

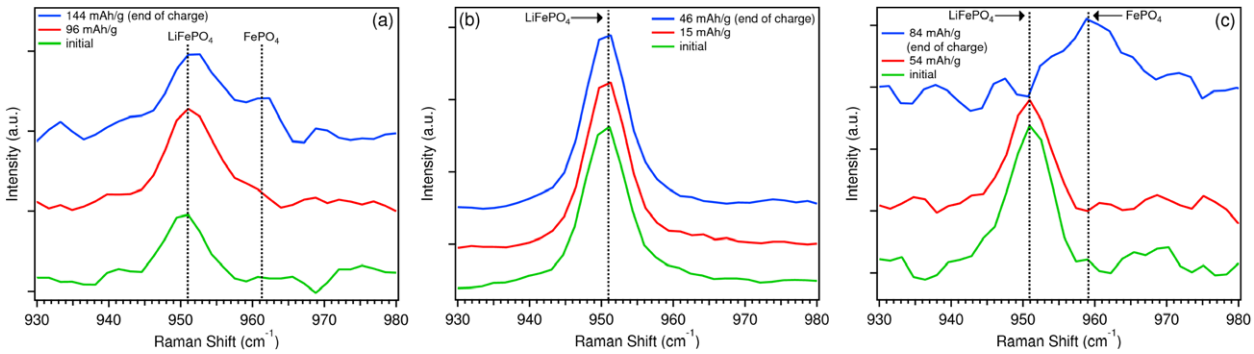

Figure 4. *In situ* Raman spectra of the PO_4^{3-} stretching region for large $LiFePO_4$ particles (a), microsphere $LiFePO_4$ without carbon coating (b) and microsphere $LiFePO_4$ with carbon coating (c).

led to either completely delithiated or intact $LiFePO_4$ after charge [20]. Our small $LiFePO_4$ was of similar size so it was less likely that both phases would coexist on the same particle. Given that the area of laser exposure ($\sim$1 μm diameter) is much larger than the small $LiFePO_4$ particles and the particles are not carbon coated for better electric contact with each other and conductors, the mixed $LiFePO_4$ phase was most likely caused by uneven electron transfer between particles.

The same *in situ* Raman experiments were conducted on larger $LiFePO_4$ nanorods and microspheres without and with carbon coating. In contrast to the small $LiFePO_4$, the sizes of large $LiFePO_4$ and microspheres are either comparable to or larger than the laser spot size. In these cases, the Raman signal was likely collected on only a few particles, which would primarily reveal the surface properties with minimal effect from inhomogeneous electron transfer between particles. During charging, all of the samples showed the similar growth of external modes at 175 and 244 cm^{-1} (results not shown). Nevertheless, because of the different surface morphology and coating, the Raman spectra in the ν_1 region varied indicating a different amount of $FePO_4$ existing at the end of charge. In figure 4, *in situ* Raman spectra in the ν_1 region of these three morphologies of $LiFePO_4$ are shown. Only spectra at initial conditions, emerging of $FePO_4$ external modes and end of charge are presented. For all three morphologies of $LiFePO_4$, the $FePO_4$ phase started to form at an early stage but $LiFePO_4$ still dominated the surface at the end of charge. For the large $LiFePO_4$ (figure 4(a)), the symmetric stretching peak of $FePO_4$ at 961 cm^{-1} appears only as a shoulder to the $LiFePO_4$ stretching at 951 cm^{-1}. Unlike the small $LiFePO_4$, because of the comparable size to laser spot size, inhomogeneous electron and mass transfer between particles alone cannot explain the large amount of $LiFePO_4$. Rather, it could be the result of defects on the surface preventing Li^+ intercalation as observed by TEM by Zaghib *et al* [25].

Another way to decrease the transport pathway for better mass and charge transfer on the surface is to make porous particles. Sun *et al* synthesized $LiFePO_4$ microspheres with an overall diameter of $\sim$2 μm, 80 nm thick nanoplates [18]. However, this material had a lower capacity (46 mAh g^{-1}), which is significantly lower than the theoretical value (170 mAh g^{-1}) and even below that of the small $LiFePO_4$. The ν_1 region of the end-of-change electrode (figure 4(b)) showed primarily $LiFePO_4$ stretching at 951 cm^{-1}. This result indicates that although porous surfaces are considered beneficial for increasing the surface/volume ratio, for low conductive materials such as $LiFePO_4$, the irregular geometry makes contact with conductive carbon additive more difficult.

The porous microspheres were coated with carbon in an attempt to overcome low conductivity. The charge capacity dramatically increased to 84 mAh g^{-1}. More importantly, as shown in figure 4(c), the ν_1 region shows that the $LiFePO_4$ stretching peak disappears completely, which confirmed the complete phase change from $LiFePO_4$ to $FePO_4$ on the surface. However, even though the surface was totally converted to $FePO_4$, the overall capacity of the microsphere does not reach the theoretical value. This suggests that conductive coatings and high surface areas may improve the charge transfer on the surface but they still cannot solve the problem of slow ionic and electronic diffusion inside the core of the microsphere. Burch and Ceder reported that the ionic diffusion along the *b*-axis of $LiFePO_4$ is subjected to defects residing in the 1D channels [2]. Those defects block charge transfer along the 1D channels in the core and the amount of defects increases with particle size.

These defects along the charge transfer channel have been also reported by Nazar *et al* [26]. In their study, site disorder in crystalline $LiFePO_4$ created anti-site defects that block Li^+ transfer along the 1D channel. The amount of anti-site defects is low ($\sim$1%) and may reside deep beneath the surface. As a result, Raman spectroscopy may not detect those anti-site defects directly. However, *in situ* Raman spectroscopy is still a powerful tool to identify the surface phase composition because it enables the detection of spontaneous surface lithiation of those charged $LiFePO_4$ as will be discussed in section 3.3.

3.3. Self-discharging of delithiated LiFePO4

Although $FePO_4$ is generally considered stable in bulk form, nanoscale forms of $FePO_4$ may be less stable due to increased surface energy. To study spontaneous lithiation, or self-discharge of $FePO_4$, the charged $LiFePO_4$ cells were rested at open circuit potential and *in situ* Raman spectra were continuously obtained to monitor the self-discharge (lithiation) process. The external modes of $FePO_4$ were

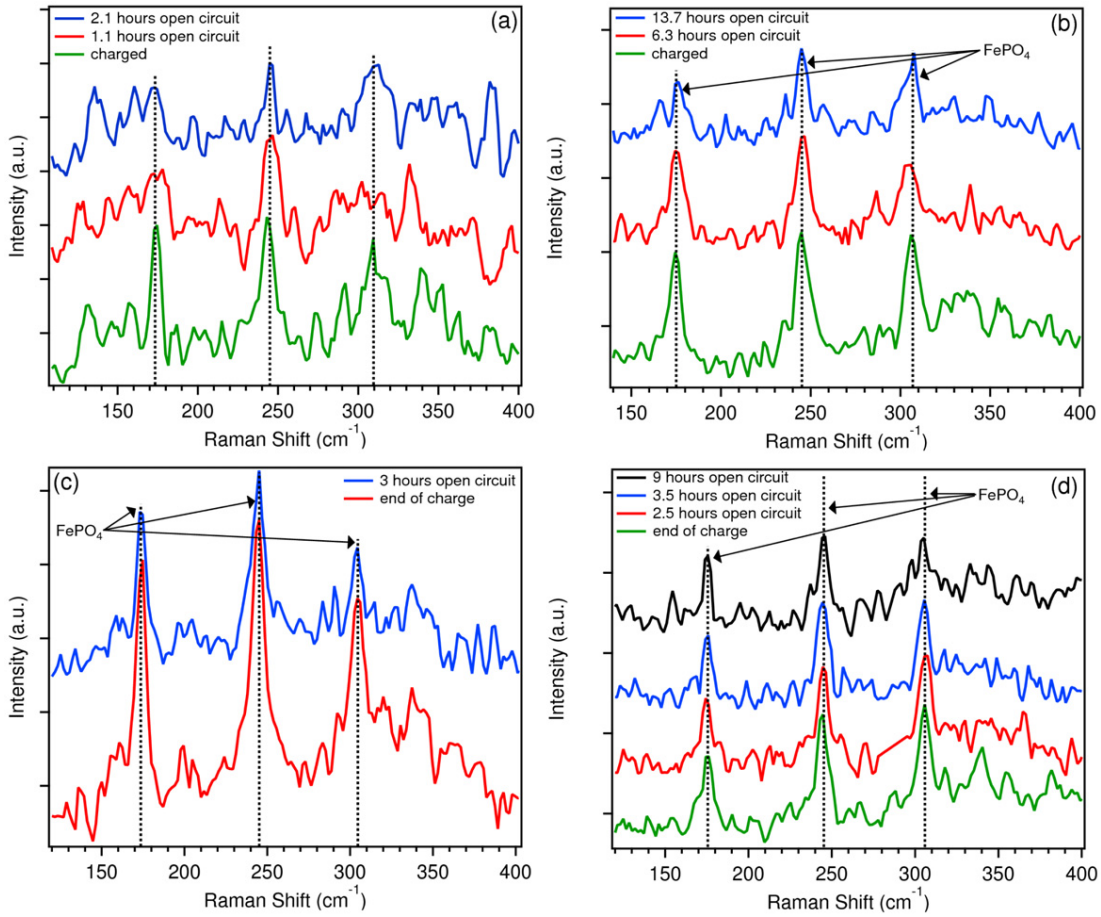

Figure 5. *In situ* Raman spectra of the external mode region of $LiFePO_4$ after charging followed by open circuit conditions for small $LiFePO_4$ nanoparticles (a), large $LiFePO_4$ particles (b), microsphere $LiFePO_4$ without carbon coating (c) and microsphere $LiFePO_4$ with carbon coating (d).

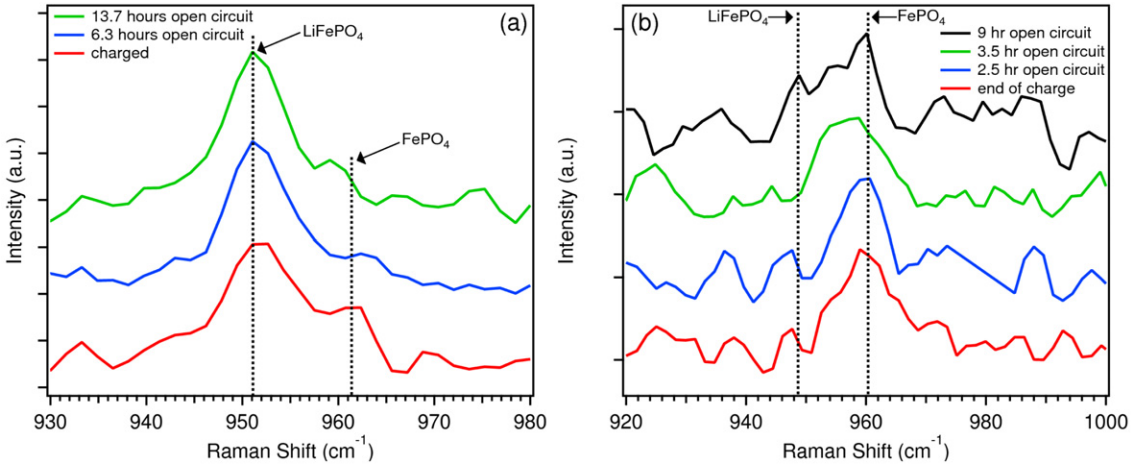

Figure 6. *In situ* Raman spectra of the PO_4^{3-} stretching region of $LiFePO_4$ after charging followed by open circuit conditions for large $LiFePO_4$ particles (a) and microsphere $LiFePO_4$ with carbon coating (b).

utilized as an indicator for the presence of $FePO_4$. Lower amount of $FePO_4$ and increasing conductivity associated with spontaneous lithiation would cause a decrease in peak intensity at 175 and 244 cm^{-1}. In addition, the relative intensity of $LiFePO_4$ and $FePO_4$ ν_1 modes were observed as the change of $LiFePO_4$/$FePO_4$ relative intensity.

Figure 5 shows the external modes of the four $LiFePO_4$ morphologies rested at open circuit potential after charging. For small $FePO_4$, the peaks at 175 and 244 cm^{-1} (figure 5(a)) started to fade after just 1 h of rest. After 2 h, the $FePO_4$ phase was barely detectable by Raman spectroscopy. Compared to the fast self-discharging of small $LiFePO_4$, the other

larger particles are all much more stable with the external modes existing for over 3 h. In the case of large $LiFePO_4$ (figure 5(b)), the $FePO_4$ external modes are still prominent after 13 h. These results indicate that smaller particles are less stable than larger particles at the surface.

To further demonstrate the surface stability of the larger particles, the $LiFePO_4$ and $FePO_4$ symmetric stretching peaks are presented in figure 6 for the two most stable particles: large particles and microspheres with carbon coating. Although the external modes do not show an obvious decrease in figure 5(b), the ν_1 mode of large $FePO_4$ at 961 cm^{-1} in figure 6(a) slowly decreases after 6 h indicating that spontaneous lithiation was still occurring, but at a considerably slower rate. Slow self-discharging was also evident for the carbon-coated microspheres as seen in figure 6(b). After 2.5 h almost no change is observed. However, after 3.5 h, the shoulder at 951 cm^{-1} begins to increase and after 9.5 h, broad peaks between 951 and 961 cm^{-1} indicate a fairly large amount of $LiFePO_4$ phase reforming. These results show that carbon coating does not significantly stabilize the high-energy surface.

4. Conclusions

Raman spectroscopy is a powerful technique to study the lithiation/delithiation related phase changes occurring at the surface of $LiFePO_4$. In this work, *in situ* Raman spectroscopy was utilized for the study of $LiFePO_4$ particles of different sizes and morphologies during charge and self-discharge with the results being compared to DFT (HSE06) calculated values. *In situ* Raman spectroscopy showed the incomplete delithiation of large $LiFePO_4$, which agrees well with the model of 1D channel blocking due to anti-site defects. Even if the larger particles had a nanostructured surface to minimize surface defects, the defects inside the core still prevent the particles from being fully delithiated. Although smaller $LiFePO_4$ particles can reduce defects and diffusion length for faster ion and electron transfer, they also destabilize the particles as indicated by faster spontaneous surface discharge. Furthermore, this reduced surface stability cannot be improved greatly by surface carbon coating.

Acknowledgments

This material is based upon work supported as part of the program 'Understanding Charge Separation and Transfer at Interfaces in Energy Materials (EFRC:CST)', an Energy Frontier Research Center funded by the US Department of Energy, Office of Science, Office of Basic Energy Sciences under Award Number DE-SC0001091. We also acknowledge the computational resources from National Energy Research Scientific Computing Center (NERSC), which is supported by the Office of Science of the US Department of Energy under Contract No. DE-AC02-05CH11231.

References

[1] Padhi A K, Nanjundaswamy K S and Goodenough J B 1997 Phospho-olivines as positive-electrode materials for rechargeable lithium batteries *J. Electrochem. Soc.* **144** 1188

[2] Malik R, Burch D, Bazant M and Ceder G 2010 Particle size dependence of the ionic diffusivity *Nano Lett.* **10** 4123–7

[3] Ferrari S, Lavall R L, Capsoni D, Quartarone E, Magistris A, Mustarelli P and Canton P 2010 Influence of particle size and crystal orientation on the electrochemical behavior of carbon-coated $LiFePO_4$ *J. Phys. Chem.* C **114** 12598–603

[4] Delacourt C, Poizot P, Levasseur S and Masquelier C 2006 Size effects on carbon-free $LiFePO_4$ powders the key to superior energy density *Electrochem. Solid State Lett.* **9** A352–5

[5] Murugan A V, Muraliganth T and Manthiram A 2008 Comparison of microwave assisted solvothermal and hydrothermal syntheses of $LiFePO_4$/C nanocomposite cathodes for lithium ion batteries *J. Phys. Chem.* C **112** 14665–71

[6] Gibot P, Casas-Cabanas M, Laffont L, Levasseur S, Carlach P, Hamelet S, Tarascon J-M and Masquelier C 2008 Room-temperature single-phase Li insertion/extraction in nanoscale $Li_{(x)}FePO_4$ *Nature Mater.* **7** 741–7

[7] Kao Y H, Tang M, Meethong N, Bai J, Carter W C and Chiang Y M 2010 Overpotential-dependent phase transformation pathways in lithium iron phosphate battery electrodes *Chem. Mater.* **22** 5845–55

[8] Andersson A S, Kalska B, Häggström L and Thomas J O 2000 Lithium extraction/insertion in $LiFePO_4$: an x-ray diffraction and Mössbauer spectroscopy study *Solid State Ion.* **130** 41–52

[9] Rodriguez M A, Van Benthem M H, Ingersoll D, Vogel S C and Reiche H M 2010 *In situ* analysis of $LiFePO_4$ batteries: signal extraction by multivariate analysis *Powder Diffr.* **25** 143–8

[10] Matsui H, Nakamura T, Kobayashi Y, Tabuchi M and Yamada Y 2010 Open-circuit voltage study on $LiFePO_4$ olivine cathode *J. Power Sources* **195** 6879–83

[11] Zhu Y and Wang C 2010 Galvanostatic intermittent titration technique for phase-transformation electrodes *J. Phys. Chem.* C **114** 2830–41

[12] Paques-Ledent M T and Tarte P 1974 Vibrational studies of olivine-type compounds 2. Orthophosphates, orthoarsenates and orthovanadates $A_IB_{IIX}VO_4$ *Spectrochim. Acta* A **30** 673

[13] Kresse G and Furthmüller J 1996 Efficiency of *ab initio* total energy calculations for metals and semiconductors using a plane-wave basis set *Comput. Mater. Sci.* **6** 15–50

[14] Kresse G and Furthmüller J 1996 Efficient iterative schemes for *ab initio* total-energy calculations using a plane-wave basis set *Phys. Rev.* B **54** 11169–86

[15] Heyd J, Scuseria G E and Ernzerhof M 2003 Hybrid functionals based on a screened Coulomb potential *J. Chem. Phys.* **118** 8207

[16] Heyd J, Scuseria G E and Ernzerhof M 2006 Erratum: hybrid functionals based on a screened Coulomb potential *J. Chem. Phys.* **118** 8207
Heyd J, Scuseria G E and Ernzerhof M 2003 *J. Chem. Phys.* **124** 219906

[17] Burba C M and Frech R 2004 Raman and FTIR spectroscopic study of Li_xFePO_4 ($0 \leq x \leq 1$) *J. Electrochem. Soc.* **151** A1032

[18] Sun C, Rajasekhara S, Goodenough J B and Zhou F 2011 Monodisperse porous $LiFePO_4$ microspheres for a high power Li-ion battery cathode *J. Am. Chem. Soc.* **133** 2132–5

[19] Burba C M, Palmer J M and Holinsworth B S 2009 Laser-induced phase changes in olivine $FePO_4$: a warning on characterizing $LiFePO_4$-based cathodes with Raman spectroscopy *J. Raman Spectrosc.* **40** 225–8

[20] Delmas C, Maccario M, Croguennec L, Le Cras F and Weill F 2008 Lithium deintercalation in $LiFePO_4$ nanoparticles via a domino-cascade model *Nature Mater.* **7** 665–71

[21] Gouveia D, Lemos V, de Paiva J, Souza Filho A, Mendes Filho J, Lala S, Montoro L and Rosolen J 2005 Spectroscopic studies of Li_xFePO_4 and $Li_xM_{0.03}Fe_{0.97}PO_4$ (M = Cr, Cu, Al, Ti) *Phys. Rev.* B **72** 024105

[22] Paraguassu W, Freire P T C, Lemos V, Lala S M, Montoro L A and Rosolen J M 2005 Phonon calculation on olivine-like $LiMPO_4$ (M = Ni, Co, Fe) and Raman scattering of the iron-containing compound *J. Raman Spectrosc.* **36** 213–20

[23] Shi S, Zhang H, Ke X, Ouyang C, Lei M and Chen L 2009 First-principles study of lattice dynamics of $LiFePO_4$ *Phys. Lett.* A **373** 4096–100

[24] Julien C M, Mauger A and Zaghib K 2011 Surface effects on electrochemical properties of nano-sized $LiFePO_4$ *J. Mater. Chem.* **21** 9955

[25] Ramana C V, Mauger A, Gendron F, Julien C M and Zaghib K 2009 Study of the Li-insertion/extraction process in $LiFePO_4/FePO_4$ *J. Power Sources* **187** 555–64

[26] Badi S-P, Wagemaker M, Ellis B L, Singh D P, Borghols W J H, Kan W H, Ryan D H, Mulder F M and Nazar L F 2011 Direct synthesis of nanocrystalline $Li_{0.90}FePO_4$: observation of phase segregation of anti-site defects on delithiation *J. Mater. Chem.* **21** 10085